ACS OMEGA

http://pubs.acs.org/journal/acsodf

Article

Dissection of the Active Ingredients and Potential Mechanism of Han-Shi-Yu-Fei-Decoction in Treating COVID-19 Based on In Vivo Substances Profiling and Clinical Symptom-Guided Network Pharmacology

Guangyang Jiao, Xiangcheng Fan, Yejian Wang, Nan Weng, Luolan Ouyang, Haoqian Wang, Sihan Pan, Doudou Huang, Jun Han, Feng Zhang,* and Wansheng Chen*

Cite This: *ACS Omega* 2022, 7, 36598−36610

Read Online

ACCESS | Metrics & More | Article Recommendations

ABSTRACT: This work was aimed to elucidate the mechanism of action of Han-Shi-Yu-Fei-decoction (HSYFD) for treating patients with mild coronavirus disease 2019 (COVID-19) based on clinical symptom-guided network pharmacology. Experimentally, an ultra-high performance liquid chromatography technique coupled with quadrupole time-of-flight mass spectrometry method was used to profile the chemical components and the absorbed prototype constituents in rat serum after its oral administration, and 11 out of 108 compounds were identified. Calculatingly, the disease targets of Han-Shi-Yu-Fei symptoms of COVID-19 were constructed through the TCMIP V2.0 database. The subsequent network pharmacology and molecular docking analysis explored the molecular mechanism of the absorbed prototype constituents in the treatment of COVID-19. A total of 42 HSYFD targets oriented by COVID-19 clinical symptom were obtained, with EGFR, TP53, TNF, JAK2, NR3C1, TH, COMT, and DRD2 as the core targets. Enriched pathway analysis yielded multiple COVID-19-related signaling pathways, such as the PI3K/AKT signaling pathway and JAK-STAT pathway. Molecular docking showed that the key compounds, such as 6-gingerol, 10-gingerol, and scopoletin, had high binding activity to the core targets like COMT, JAK2, and NR3C1. Our work also verified the feasibility of clinical symptom-guided network pharmacology analysis of chemical compounds, and provided a possible agreement between the points of views of traditional Chinese medicine and western medicine on the disease.

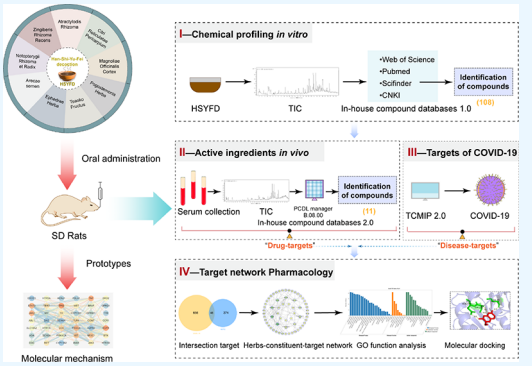

1. INTRODUCTION

Since the outbreak of COVID-19 in 2019, it has stayed a global public health concern that has not yet been effectively resolved, posing a serious threat to human health and economic development.[1] Traditional Chinese medicine (TCM) has played a vital role in COVID-19 prevention and treatment. It has been listed in the "Diagnosis and Treatment Plan for COVID-19 Infection", version 3, issued by the National Health Commission of the People's Republic of China.[2] Significantly, the combination of TCM and western medicine has led to significant achievements in the battle against COVID-19.[3]

It is well accepted that COVID-19 may evolve in four (overlapping) phases, from mild to moderate to severe to critical, which is staged by the clinical symptoms. Treatment of patients in mild and moderate stages is of utmost importance because about 14% of patients can progress to severe stage in only 1 week.[4] Of note, both TCM and western medicine systems have a general agreement on this point.[5] The typical clinical symptoms, including fever, cough, abnormality of the pharynx, fatigue, anergy, dyspnea, abnormality of the stomach, nausea, vomiting, diarrhea, abnormality of the tongue, and abnormality of the vasculature, were interpreted as "Han" and "Shi" that were blocked in the lung, according to the theory of TCM. Therefore, the typical recommended TCM recipe was "Han-Shi-Yu-Fei decoction (HSYFD)". It consists of Atractylodis rhizoma [AR; *Atractylodes lancea* (Thunb.) DC.], Citri reticulatae pericarpium (CRP; *Citrus reticulata* Blanco), Magnoliae officinalis cortex (MOC; *Magnolia officinalis* Rehd. et Wils.), Pogostemonis Herba [PH; *Pogostemon cablin* (Blanco) Benth.], Tsaoko Fructus (TF; *Amomum tsao-ko* Crevost et Lemaire), Ephedrae Herba (EH; *Ephedra sinica* Stapf), Notopterygii rhizoma et Radix (NRR; *Notopterygium incisum* Ting ex H.T. Chang), Arecae semen (AS; *Areca catechu*

Received: July 20, 2022
Accepted: September 28, 2022
Published: October 7, 2022

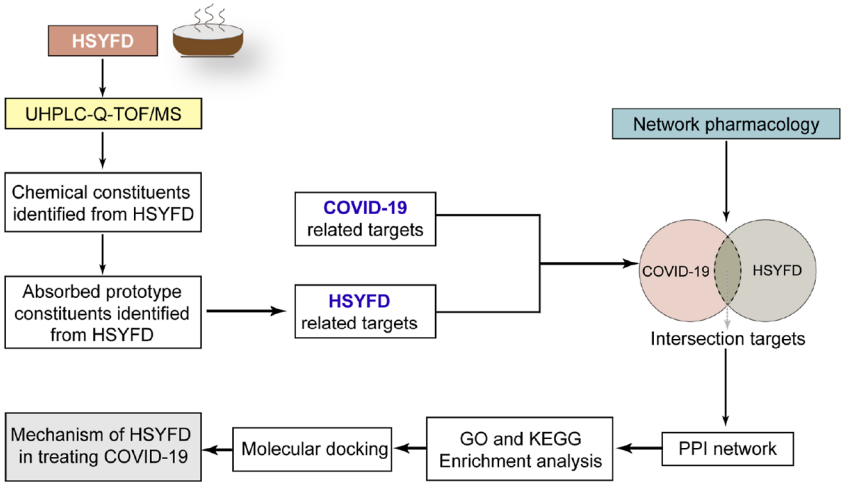

Figure 1. Whole framework of this study.

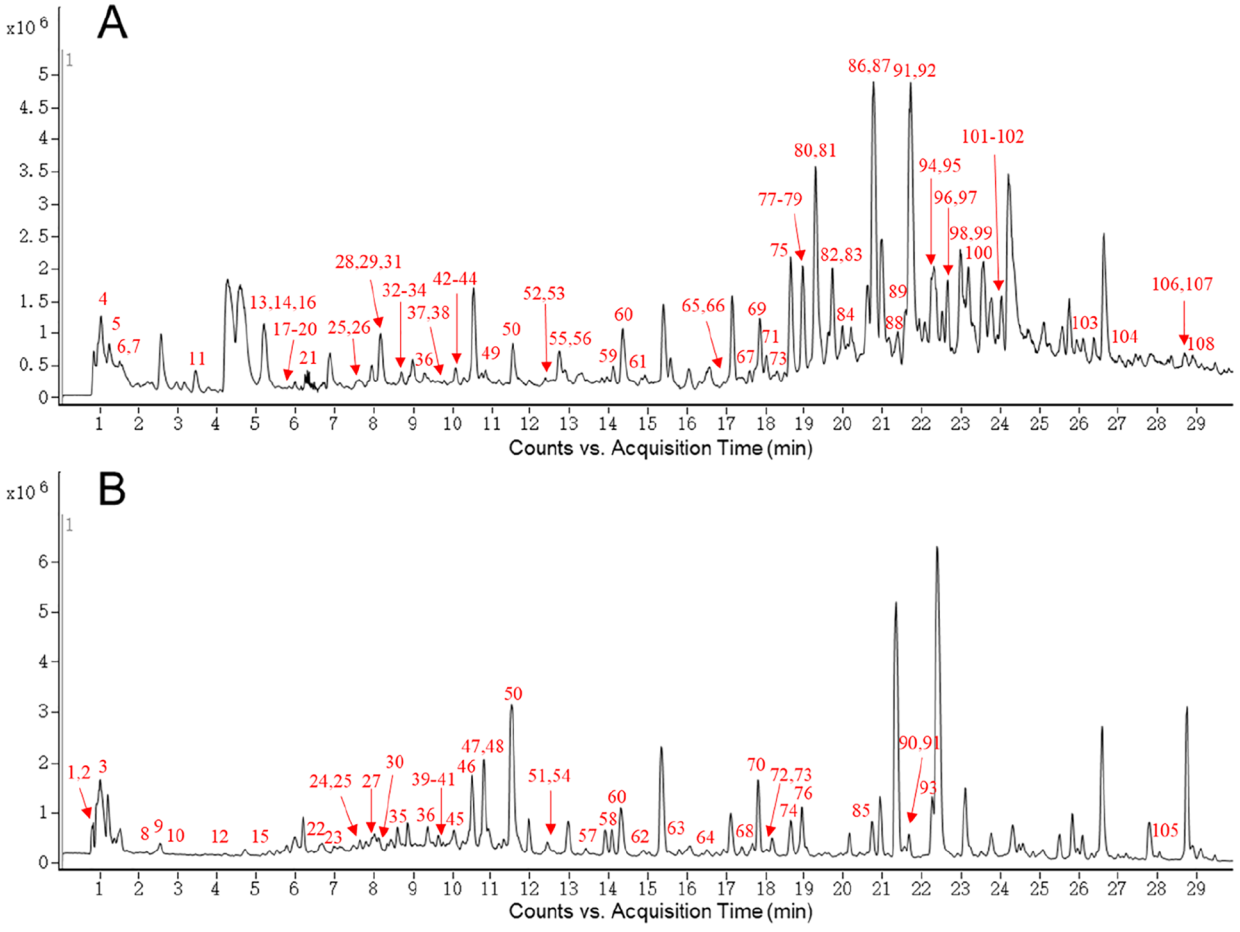

Figure 2. Extract ion chromatograms of HSYFD. (A) Positive mode and (B) negative mode.

L.), and Zingiberis rhizoma Recens (ZRR; *Zingiber officinale* Rosc.).[6] However, its active compounds and therapeutic mechanisms have not been studied yet.

According to the current network of pharmacology research and a few in vitro experiments, the mechanism of TCM in COVID-19 is a multi-component, multi-target, and multi-pathway, which exhibits the functions of combating viral infections, immune regulation, amelioration of lung injury and fibrosis, and protection of target organs.[7,8] However, most of the network pharmacology research studies were guided by the disease targets.[9] As the COVID-19 patients were staged by the clinical symptoms, which were associated with the progression from mild to moderate COVID-19 illness to severe or critical status, it is an effective way to force mechanism study by the disease symptom-guided network pharmacology.

In this study, an ultra-high performance liquid chromatography coupled with quadrupole time-of-flight mass spectrometry (UHPLC−Q-TOF-MS) method was used to identify the chemical components of HSYFD in vitro and then discriminate the blood-absorbing constituents, which were involved in the

https://doi.org/10.1021/acsomega.2c04589
ACS Omega 2022, 7, 36598−36610

Table 1. Identification of Compounds in HSYFD by UHPLC−Q-TOF-MS[b]

no.	RT (min)	mode	average m/z	adduct type	MS/MS spectrum	error (ppm)	formula	compound	category	source
1	0.868	ESI−	154.0616	$[M-H]^-$	137.0343	−3.50	$C_6H_9N_3O_2$	histidine	amino acids	AS
2	0.868	ESI−	173.1042	$[M-H]^-$	131.0798	−2.18	$C_6H_{14}N_4O_2$	arginine	amino acids	AS
3	0.936	ESI−	245.0435	$[M-H]^-$	215.0329	−4.47	$C_{13}H_{10}O_5$	isopimpinellin	coumarins	NRR
4	1.059	ESI+	118.0862	$[M+H]^+$	100.0450	−0.26	$C_5H_{11}NO_2$	valine	amino acids	AS
5	1.286	ESI+	182.0826	$[M+H]^+$	165.0619, 136.0723, 123.0544	8.54	$C_9H_{11}NO_3$	tyrosine	amino acids	AS
6	1.434	ESI+	132.102	$[M+H]^+$	115.0422	1.04	$C_6H_{13}NO_2$	leucine	amino acids	AS
7	1.582	ESI+	166.1229	$[M+H]^+$	152.108, 132.1013, 117.0748	1.30	$C_{10}H_{15}NO$	pseudoephedrine	alkaloids	EH
8	2.188	ESI-	164.0714	$[M-H]^-$	164.0174, 147.0510	−1.88	$C_9H_{11}NO_2$	L-phenylalanine	amino acids	AR
9	2.416	ESI−	167.0348	$[M-H]^-$	123.0487	−1.60	$C_8H_8O_4$	vanillic acid	phenols	NRR, PH, MOC, AS, AR, CRP, TF
10	2.906	ESI−	153.0191	$[M-H]^-$	109.0302	−1.89	$C_7H_6O_4$	gentisic acid	phenols	TF
11	3.449	ESI+	152.1073	$[M+H]^+$	134.0970, 117.0701	2.05	$C_9H_{13}NO$	norephedrine	alkaloids	EH
12	4.169	ESI−	203.0832	$[M-H]^-$	142.0698, 116.0506	2.45	$C_{11}H_{12}N_2O_2$	D-tryptophan	amino acids	AR
13	5.202	ESI+	180.1389	$[M+H]^+$	162.1280, 117.0721	3.12	$C_{11}H_{17}NO$	methylephedrine	alkaloids	EH
14	5.214	ESI+	135.0808	$[M+H]^+$	119.0816	1.06	$C_9H_{10}O$	chavicol	phenols	MOC
15	5.365	ESI−	188.0354	$[M-H]^-$	144.0439, 131.0366	−0.84	$C_{10}H_7NO_3$	kynurenic acid	amino acids	EH
16	5.373	ESI+	166.1227	$[M+H]^+$	166.1226, 148.1117	0.20	$C_{10}H_{15}NO$	ephedrine	alkaloids	EH
17	5.612	ESI+	192.1023	$[M+H]^+$	146.0515, 133.1011, 105.0667	1.43	$C_{11}H_{13}NO_2$	ephedroxane	alkaloids	EH
18	5.817	ESI+	139.0392	$[M+H]^+$	139.0386, 121.0506	1.45	$C_7H_6O_3$	4-hydroxybenzoic acid	phenols	AS, TF
19	5.840	ESI+	195.0655	$[M+H]^+$	177.0546,145.0513	3.08	$C_{10}H_{10}O_4$	ferulic acid	phenylpropanoids	AS, EH
20	5.977	ESI+	233.1535	$[M+H]^+$	233.1535, 215.142, 187.1429	0.17	$C_{15}H_{20}O_2$	atractylenolide II	sesquiterpenoids	AR
21	6.227	ESI+	355.1021	$[M+H]^+$	193.087, 163.038	−0.59	$C_{16}H_{18}O_9$	chlorogenic acid	caffeoylquinic acids	NRR, EH, MOC
22	6.617	ESI−	179.0348	$[M-H]^-$	135.0446	−1.26	$C_9H_8O_4$	caffeic acid	phenylpropanoids	MOC, EH, CRP
23	7.015	ESI−	369.0827	$[M-H]^-$	207.0209	0.06	$C_{16}H_{18}O_{10}$	fraxin	coumarins	NRR
24	7.539	ESI−	153.0193	$[M-H]^-$	135.0438, 109.0305	−0.35	$C_7H_6O_4$	protocatechuic acid	hydroxybenzoic acid derivatives	TF, AS
25	7.653	ESI−	289.0716	$[M-H]^-$	151.0384, 137.0238, 121.0239, 109.0290	−0.40	$C_{15}H_{14}O_6$	epicatechin	flavonoids	EH, AS, TF
	7.718	ESI+	291.0868	$[M+H]^+$	123.1151	2.65	$C_{15}H_{14}O_6$	epicatechin		
26	7.866	ESI+	149.0606	$[M+H]^+$	131.0482, 103.0549	4.83	$C_9H_8O_2$	cinnamic acid	phenylpropanoids	EH
27	8.017	ESI−	163.04	$[M-H]^-$	163.0405, 145.0258, 119.0363	−1.47	$C_9H_8O_3$	*p*-coumaric acid	phenols	MOC, CRP, NRR
28	8.049	ESI+	223.0603	$[M+H]^+$	177.0563, 163.0385, 151.0368, 121.0507	1.02	$C_{11}H_{10}O_5$	isofraxidin	coumarins	NRR
29	8.071	ESI+	595.1652	$[M+H]^+$	287.1398, 255.0938	−0.85	$C_{27}H_{30}O_{15}$	lonicerin	flavonoids	CRP
30	8.120	ESI−	151.0399	$[M-H]^-$	151.0399, 135.0448, 119.0384	−1.03	$C_8H_8O_3$	vanillin	phenols	EH
31	8.174	ESI+	342.1712	$[M]^+$	342.171, 297.1169	3.20	$C_{20}H_{23}NO_4^+$	magnoflorine	alkaloids	MOC
32	8.584	ESI+	137.1323	$[M+H]^+$	109.0993	−1.70	$C_{10}H_{16}$	camphene	monoterpenoids	PH
33	8.652	ESI+	765.2214	$[M+Na]^+$	581.1885, 435.1274	−0.09	$C_{33}H_{42}O_{19}$	narirutin-4′-glucoside	flavonoid-7-o-glycosides	CRP
34	8.709	ESI+	330.1704	$[M+H]^+$	330.1706, 192.113	1.29	$C_{19}H_{23}NO_4$	reticuline	alkaloids	MOC
35	8.860	ESI−	623.1987	$[M-H]^-$	461.1522, 135.0454	0.65	$C_{29}H_{36}O_{15}$	acteoside	steroids	MOC, PH
36	9.235	ESI−	191.0349	$[M-H]^-$	175.0375, 161.0275, 147.0442	0.43	$C_{10}H_8O_4$	scopoletin	coumarins	NRR
	9.301	ESI+	193.0501	$[M+H]^+$	163.0572, 149.0595	3.10	$C_{10}H_8O_4$	scopoletin		
37	9.608	ESI+	197.117	$[M+H]^+$	179.1049, 133.1011	0.88	$C_{11}H_{16}O_3$	loliolide	benzofurans	PH

https://doi.org/10.1021/acsomega.2c04589
ACS Omega 2022, 7, 36598−36610

Table 1. continued

no.	RT (min)	mode	average m/z	adduct type	MS/MS spectrum	error (ppm)	formula	compound	category	source
38	9.608	ESI+	153.1271	$[M + H]^+$	153.1273, 135.117, 121.051, 107.0855	−0.75	$C_{10}H_{16}O$	citral	monoterpenoids	CRP
39	9.645	ESI−	609.1458	$[M - H]^-$	301.0360	0.34	$C_{27}H_{30}O_{16}$	rutin	flavonoids	TF, CRP
40	9.656	ESI−	577.1563	$[M - H]^-$	431.0955, 269.0382	0.11	$C_{27}H_{30}O_{14}$	rhoifolin	flavonoids	CRP
41	9.782	ESI−	595.1651	$[M - H]^-$	287.0561	−2.37	$C_{27}H_{32}O_{15}$	neoeriocitrin	flavonones	CRP
42	9.950	ESI+	356.1855	$[M + H]^+$	325.1066	−0.57	$C_{21}H_{25}NO_4$	glaucine	quinolines	MOC
43	10.007	ESI+	223.1329	$[M + H]^+$	205.1200, 187.0773, 163.0657	0.07	$C_{13}H_{18}O_3$	dehydrovomifoliol	sesquiterpenoids	MOC
44	10.075	ESI+	268.134	$[M + H]^+$	251.1082	2.87	$C_{17}H_{17}NO_2$	asimilobine	alkaloids	MOC
45	10.100	ESI−	447.0937	$[M - H]^-$	285.0406	1.48	$C_{21}H_{20}O_{11}$	isoorientin	flavonoid c-glycosides	CRP
46	10.510	ESI−	453.141	$[M + HCOO]^-$	227.071	0.50	$C_{20}H_{24}O_9$	nodakenin	coumarins	NRR
47	10.727	ESI−	463.0885	$[M - H]^-$	300.0224, 151.0375	1.07	$C_{21}H_{20}O_{12}$	quercetin-3-galactoside	flavonoid-3-o-glycosides	EH
48	10.806	ESI−	579.172	$[M - H]^-$	459.1124, 271.0623	−0.18	$C_{27}H_{32}O_{14}$	naringin	flavonones	CRP
49	10.895	ESI+	209.0815	$[M + H]^+$	177.0532, 149.1006, 121.0507	3.51	$C_{11}H_{12}O_4$	sinapic aldehyde	phenols	MOC
50[a]	11.501	ESI−	609.1827	$[M - H]^-$	609.1822, 325.0666, 301.0739,	0.17	$C_{28}H_{34}O_{15}$	hesperidin	flavonones	PH, EH, CRP
	11.544	ESI+	611.1975	$[M + H]^+$	465.1393, 303.0863, 177.0554	0.64	$C_{28}H_{34}O_{15}$	hesperidin		
51	12.468	ESI−	269.0464	$[M - H]^-$	269.0464, 117.0246	2.70	$C_{15}H_{10}O_5$	apigenin	flavonoids	PH, CRP, EH
52	12.648	ESI+	276.0659	$[M + H]^+$	248.0742	1.97	$C_{17}H_9NO_3$	liriodenine	alkaloids	MOC
53	12.659	ESI+	155.1424	$[M + H]^+$	137.1323, 107.0852	−4.65	$C_{10}H_{18}O$	α-terpineol	monoterpenoids	EH
54	12.730	ESI−	295.0982	$[M - H]^-$	267.0660, 151.0406	−1.56	$C_{18}H_{16}O_4$	obovatal	neolignans	MOC
55	12.750	ESI+	266.1184	$[M + H]^+$	249.0983, 236.1679	3.04	$C_{17}H_{15}NO_2$	anonaine	alkaloids	MOC
56	12.898	ESI+	280.1341	$[M + H]^+$	249.0909	2.94	$C_{18}H_{17}NO_2$	roemerine	alkaloids	MOC
57	13.391	ESI−	301.0355	$[M - H]^-$	271.0246, 151.0048,	0.61	$C_{15}H_{10}O_7$	quercetin	flavonoids	EH, AS, TF
58	13.914	ESI−	593.1874	$[M - H]^-$	285.0774	0.34	$C_{28}H_{34}O_{14}$	poncirin	flavonones	CRP
59	14.117	ESI+	247.0974	$[M + H]^+$	177.0551, 147.0453	3.78	$C_{14}H_{14}O_4$	columbianetin	coumarins	NRR
60	14.301	ESI−	491.1195	$[M + HCOO]^-$	283.0613, 133.0309	−0.30	$C_{22}H_{22}O_{10}$	acacetin-7-glucoside	flavonoid-7-*O*-glycosides	PH
	14.356	ESI+	447.1304	$[M + H]^+$	285.0746	3.82	$C_{22}H_{22}O_{10}$	acacetin-7-glucoside		
61	14.857	ESI+	151.1117	$[M + H]^+$	151.1116, 133.1028, 107.0849	1.05	$C_{10}H_{14}O$	2-(4-methylphenyl)propan-2-ol	phenylpropanes	MOC
62	14.893	ESI−	726.3825	$[M - H]^-$	708.3709, 696.3708	−1.45	$C_{36}H_{53}N_7O_9$	citrusin III	alkaloids	CRP
63	15.759	ESI−	329.0666	$[M - H]^-$	313.0718, 283.0612, 253.0486	−0.49	$C_{17}H_{14}O_7$	ombuin	flavonoids	PH
64	16.578	ESI−	359.0771	$[M - H]^-$	283.0635	−0.53	$C_{16}H_{12}O_6$	diosmetin	flavonoids	NRR
65	16.951	ESI+	353.2293	$[M + Na]^+$	261.1767	−2.11	$C_{18}H_{34}O_5$	tianshic acid	fatty acids	PH
66	17.031	ESI+	251.1983	$[M + Na]^+$	229.1246, 209.1115, 121.0512	1.49	$C_{14}H_{28}O_2$	myristic acid	fatty acids	AS
67	17.691	ESI+	231.1022	$[M + H]^+$	175.0391, 147.1164	2.80	$C_{14}H_{14}O_3$	osthenol	7-hydroxycoumarins	NRR
68	17.762	ESI−	279.1029	$[M - H]^-$	239.0726, 133.0188	0.91	$C_{18}H_{16}O_3$	magnaldehyde B	neolignans	MOC
69	17.794	ESI+	343.1185	$[M + H]^+$	287.0955, 163.0733	1.97	$C_{19}H_{18}O_6$	4′,5,7,8-tetramethoxyflavone	flavonoids	CRP
70	17.808	ESI−	283.0618	$[M - H]^-$	283.0619, 268.0355	1.80	$C_{16}H_{12}O_5$	wogonin	flavonoids	AR
71	17.999	ESI+	205.1956	$[M + H]^+$	177.0919, 163.0751,149.1320	2.44	$C_{15}H_{24}$	α-bulnesene	sesquiterpenoids	PH
72	18.092	ESI−	300.0878	$[M - H]^-$	270.0464	1.13	$C_{16}H_{15}NO_5$	citpressine I	acridones	CRP
73	18.195	ESI−	285.0772	$[M - H]^-$	201.0217	1.73	$C_{16}H_{14}O_5$	(R)-pabulenol	psoralens	NRR
	18.386	ESI+	287.092	$[M + H]^+$	215.0699, 203.0333	2.37	$C_{16}H_{14}O_5$	(R)-pabulenol		
74	18.434	ESI−	343.0831	$[M - H]^-$	283.0617	1.72	$C_{18}H_{16}O_7$	pachypodol	flavonoids	PH
75	18.640	ESI+	425.121	$[M + Na]^+$	403.1399, 375.1068, 287.0838	3.76	$C_{21}H_{22}O_8$	nobiletin	flavonoids	CRP

https://doi.org/10.1021/acsomega.2c04589
ACS Omega 2022, 7, 36598−36610

Table 1. continued

no.	RT (min)	mode	average m/z	adduct type	MS/MS spectrum	error (ppm)	formula	compound	category	source
76	18.867	ESI−	311.129	$[M + HCOO]^-$	249.0932, 223.0723	0.97	$C_{18}H_{18}O_2$	honokiol	lignans	MOC
77	18.898	ESI+	221.1901	$[M + H]^+$	203.0343, 177.0913, 163.0734, 107.0848	0.53	$C_{15}H_{24}O$	(−)-caryophyllene oxide	sesquiterpenoids	MOC
78	18.955	ESI+	312.2175	$[M + NH_4]^+$	259.1674, 163.0732, 137.0595	3.34	$C_{17}H_{26}O_4$	6-gingerol	gingerols	ZRR
79[a]	18.960	ESI+	277.181	$[M + H]^+$	119.0849, 107.0847	4.53	$C_{17}H_{24}O_3$	6-shogaol	phenylacetaldehydes	ZRR
80	19.126	ESI+	315.0872	$[M + H]^+$	300.2190, 163.1471	3.20	$C_{17}H_{14}O_6$	kumatakenin	flavonoids	PH
81	19.319	ESI+	274.2744	$[M + NH_4]^+$	211.0343	1.48	$C_{16}H_{32}O_2$	palmitic acid	fatty acids	AR
82	19.661	ESI+	299.1652	$[M + H]^+$	217.0758, 163.0728	2.74	$C_{19}H_{22}O_3$	ostruthin	coumarins	NRR
83	19.706	ESI+	395.1111	$[M + Na]^+$	343.0986	4.04	$C_{20}H_{20}O_7$	tangeretin	flavonoids	CRP
84	20.036	ESI+	287.0925	$[M + H]^+$	203.0346	3.94	$C_{16}H_{14}O_5$	pabulenol	psoralens	NRR
85[a]	20.720	ESI−	353.1397	$[M - H]^-$	201.0195	0.41	$C_{21}H_{22}O_5$	notopterol	coumarins	NRR
86	20.754	ESI+	203.0346	$[M + H]^+$	159.0803, 147.0402, 133.0973	3.42	$C_{11}H_6O_4$	xanthotoxol	8-hydroxypsoralens	NRR
87	20.754	ESI+	255.0658	$[M + H]^+$	255.0659, 121.0512	2.62	$C_{15}H_{10}O_4$	chrysophanol	anthraquinones	AS
88	21.596	ESI+	229.0865	$[M + H]^+$	135.0478, 119.0823	2.62	$C_{14}H_{12}O_3$	*trans*-resveratrol	phenols	AS
89	21.642	ESI+	137.0597	$[M + H]^+$	137.0597, 109.0648	0.78	$C_8H_8O_2$	4-methoxybenzaldehyde	benzoyl derivatives	TF
90	21.667	ESI−	201.0195	$[M - H]^-$	177.0194, 133.024, 117.029	0.10	$C_{11}H_6O_4$	bergaptol	5-hydroxypsoralens	NRR
91	21.667	ESI−	269.0819	$[M - H]^-$	201.0194	−0.3	$C_{16}H_{14}O_4$	imperatorin	psoralens	NRR
	21.710	ESI+	293.0792	$[M + Na]^+$	203.0349, 175.0397	3.70	$C_{16}H_{14}O_4$	imperatorin		
92	21.824	ESI+	137.1324	$[M + H]^+$	137.0567, 121.0509, 109.0652	−1.05	$C_{10}H_{16}$	terpinolene	monoterpenes	EH
93	22.214	ESI−	315.2539	$[M + HCOO]^-$	269.0765, 251.1129, 225.0919	−0.87	$C_{17}H_{34}O_2$	heptadecanoic acid	fatty acids	AS
94	22.632	ESI+	249.149	$[M + H]^+$	231.1382, 203.1778	2.46	$C_{15}H_{20}O_3$	atractylenolide III	sesquiterpenoids	AR
95	22.678	ESI+	245.1903	$[M + Na]^+$	209.1785, 195.1726,	8.99	$C_{15}H_{26}O$	hinesol	sesquiterpenoids	AR
96	22.769	ESI+	285.0767	$[M + H]^+$	239.1099, 135.0434	2.66	$C_{16}H_{12}O_5$	physcion	anthraquinones	AS
97	22.837	ESI+	293.2107	$[M + H]^+$	275.1944, 137.0578	−2.04	$C_{18}H_{28}O_3$	7-paradol	paradols	ZRR
98	23.224	ESI+	231.1387	$[M + H]^+$	231.1387, 213.1356, 185.1325, 105.064	3.44	$C_{15}H_{18}O_2$	atractylenolide I	sesquiterpenoids	AR
99	23.258	ESI+	279.2324	$[M + H]^+$	261.1824, 233.0831	1.70	$C_{18}H_{30}O_2$	linolenic acid	fatty acids	AS
100	23.725	ESI+	203.1799	$[M + H]^+$	161.1316, 119.0852, 105.0696	2.05	$C_{15}H_{22}$	curcumene	sesquiterpenoids	AR
101	23.896	ESI+	351.2527	$[M + H]^+$	177.0906, 145.0663, 137.0601	−0.91	$C_{21}H_{34}O_4$	10-gingerol	gingerols	ZRR
102	23.930	ESI+	305.2112	$[M + H]^+$	137.0598	0.09	$C_{19}H_{28}O_3$	8-shogaol	shogaols	ZRR
103	25.934	ESI+	329.1751	$[M + H]^+$	193.0497, 163.0758	1.22	$C_{20}H_{24}O_4$	5-geranyloxy-7-methoxycoumarin	terpene lactones	NRR
104	26.935	ESI+	305.2463	$[M + Na]^+$	135.1154, 121.0524, 107.0824	6.91	$C_{18}H_{34}O_2$	oleic acid	fatty acids	AS
105	28.065	ESI−	487.3214	$[M - H]^-$	279.0956	−1.11	$C_{33}H_{44}O_3$	eudesmagnolol	neolignans	MOC
106	28.689	ESI+	527.3136	$[M + Na]^+$	135.1176	1.98	$C_{33}H_{44}O_4$	eudesobovatol A	neolignans	MOC
107	28.689	ESI+	205.1952	$[M + H]^+$	205.1955, 149.133, 123.1162, 109.1006	0.47	$C_{15}H_{24}$	farnesene	sesquiterpenoids	EH
108	28.928	ESI+	379.2845	$[M + H]^+$	343.2225, 137.0608	0.97	$C_{23}H_{38}O_4$	12-gingerol	gingerols	ZRR

[a]The results were identified by the standards. [b]MOC: Magnoliae Officinalis Cortex; EH: *Ephedrae Herba*; TF: *Tsaoko Fructus*; AR: *Atractylodis Rhizoma*; PH: *Pogostemonis Herba*; ZRR: Zingiberis Rhizoma Recens; CRP: Citri Reticulatae Pericarpium; AS: *Arecae Semen*; NRR: Notopterygii Rhizoma et Radix.

https://doi.org/10.1021/acsomega.2c04589
ACS Omega 2022, 7, 36598−36610

Table 2. Identification of Prototype Constituents of HSYFD in Rat Serum by UHPLC−Q-TOF-MS[a]

no.	tR (min)	identification	average m/z	error (ppm)	adduct type	formula	source
1	0.759	histidine	154.0606	−0.21	$[M-H]^-$	$C_6H_9N_3O_2$	AS
2	3.658	norephedrine	152.1059	−6.3	$[M+H]^+$	$C_9H_{13}NO$	EH
3	6.058	4-hydroxybenzoic acid	139.0398	1.54	$[M+H]^+$	$C_7H_6O_3$	TF, AS
4	8.114	*p*-coumaric acid	209.0454	−5.94	$[M-H]^-$	$C_9H_8O_3$	MOC, CRP, NRR
5	9.211	scopoletin	193.0507	3.10	$[M+H]^+$	$C_{10}H_8O_4$	NRR
6	9.574	loliolide	197.1171	−0.98	$[M+H]^+$	$C_{11}H_{16}O_3$	PH
7	12.660	anonaine	266.1179	0.55	$[M+H]^+$	$C_{17}H_{15}NO_2$	MOC
8	18.813	6-gingerol	293.1740	0.57	$[M-H]^-$	$C_{17}H_{26}O_4$	ZRR
9	19.024	kumatakenin	315.0854	−3.48	$[M+H]^+$	$C_{17}H_{14}O_6$	PH
10	22.532	hinesol	223.2051	3.04	$[M+H]^+$	$C_{15}H_{26}O$	AR
11	24.013	10-gingerol	373.2312	−2.81	$[M+Na]^+$	$C_{21}H_{34}O_4$	ZRR

[a]MOC: Magnoliae officinalis cortex; EH: *Ephedrae Herba*; TF: *Tsaoko fructus*; AR: *Atractylodis rhizoma*; PH: *Pogostemonis Herba*; ZRR: Zingiberis rhizoma Recens; CRP: Citri reticulatae pericarpium; AS: *Arecae semen*; NRR: Notopterygii rhizoma et Radix.

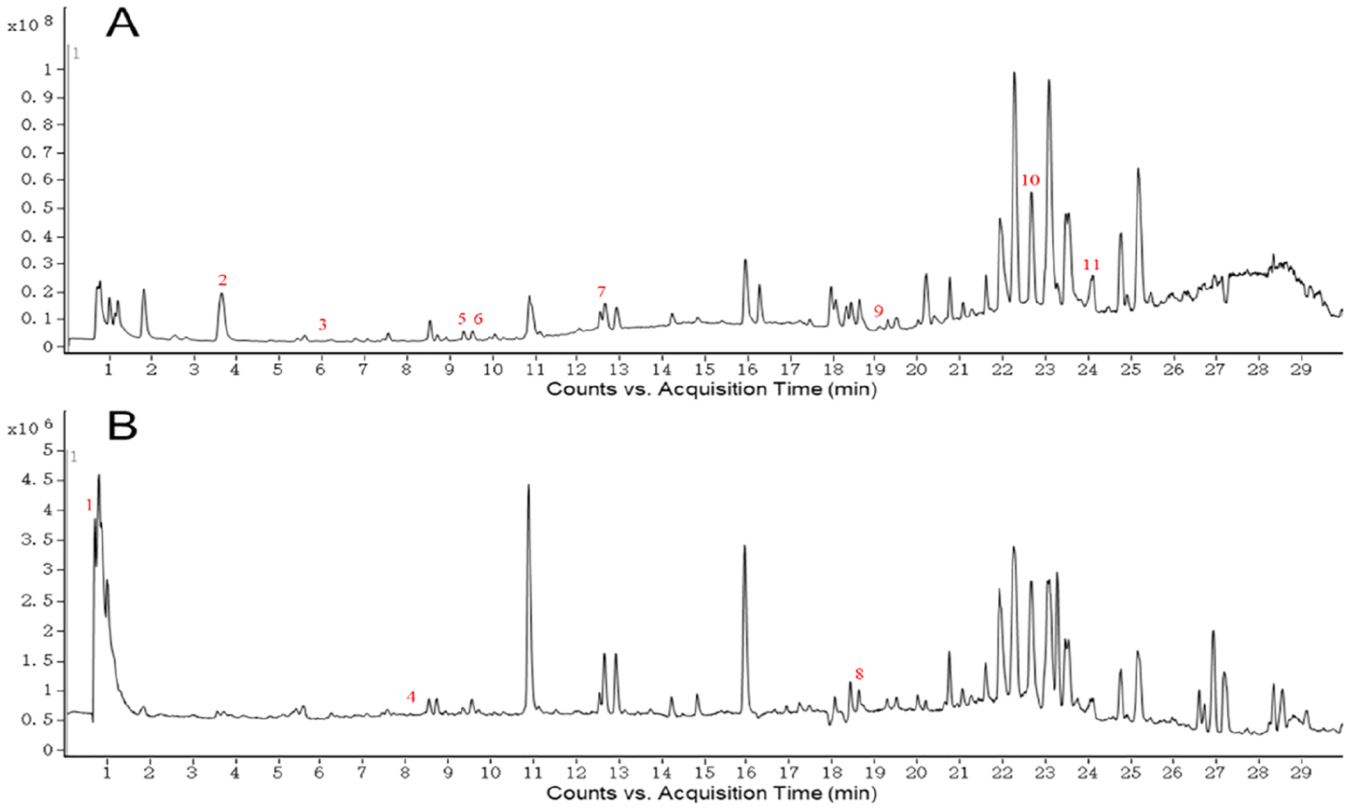

Figure 3. Extract ion chromatograms of HSYFD in the serum of rats. (A) Positive mode and (B) negative mode.

subsequent network pharmacology analysis and molecular docking techniques (Figure 1).[10,11] This strategy, based on a UHPLC−Q-TOF-MS method combined with network pharmacology, can decrease false-positive results for the TCM which should be orally administered and could be widely applied to discover phytochemical or biomolecular evidence with distinct potential functional basis. Our work provides meaningful data for further pharmacological study of HSYFD in the treatment of COVID-19.

2. RESULTS

2.1. Optimization of UHPLC−Q-TOF-MS Conditions. The separation of the chemical constituents was performed on a Waters ACQUITY UPLC BEH C18 column (2.1 × 100 mm, 1.7 μm) by gradient elution with a mobile phase (phase A: 0.1% aqueous formic acid solution and phase B: acetonitrile solution).[12,13] The chromatographic peaks were well separated and distributed in the total ion chromatogram (TIC) when the elution time was set at 30 min.

2.2. Identification of Compounds in HSYFD. The TICs of HSYFD in both positive and negative modes are shown in Figure 2. This was the first step to construct an in-house compound database 1.0 (HSYFD) by combining the compound information. The available information including the chemical name, formula, and accurate molecular weight, by searching the reference databases (such as PubMed, SciFinder, Web of Science, and CNKI), and generated the two-dimensional data (*m*/*z*-compounds) for the chemical compounds from all the herbs from HSYFD. Second, compounds were characterized by the systematically matched information in Agilent MassHunter Qualitative Analysis 10.0 software by the function "find by formula". An average mass error of

https://doi.org/10.1021/acsomega.2c04589
ACS Omega 2022, 7, 36598−36610

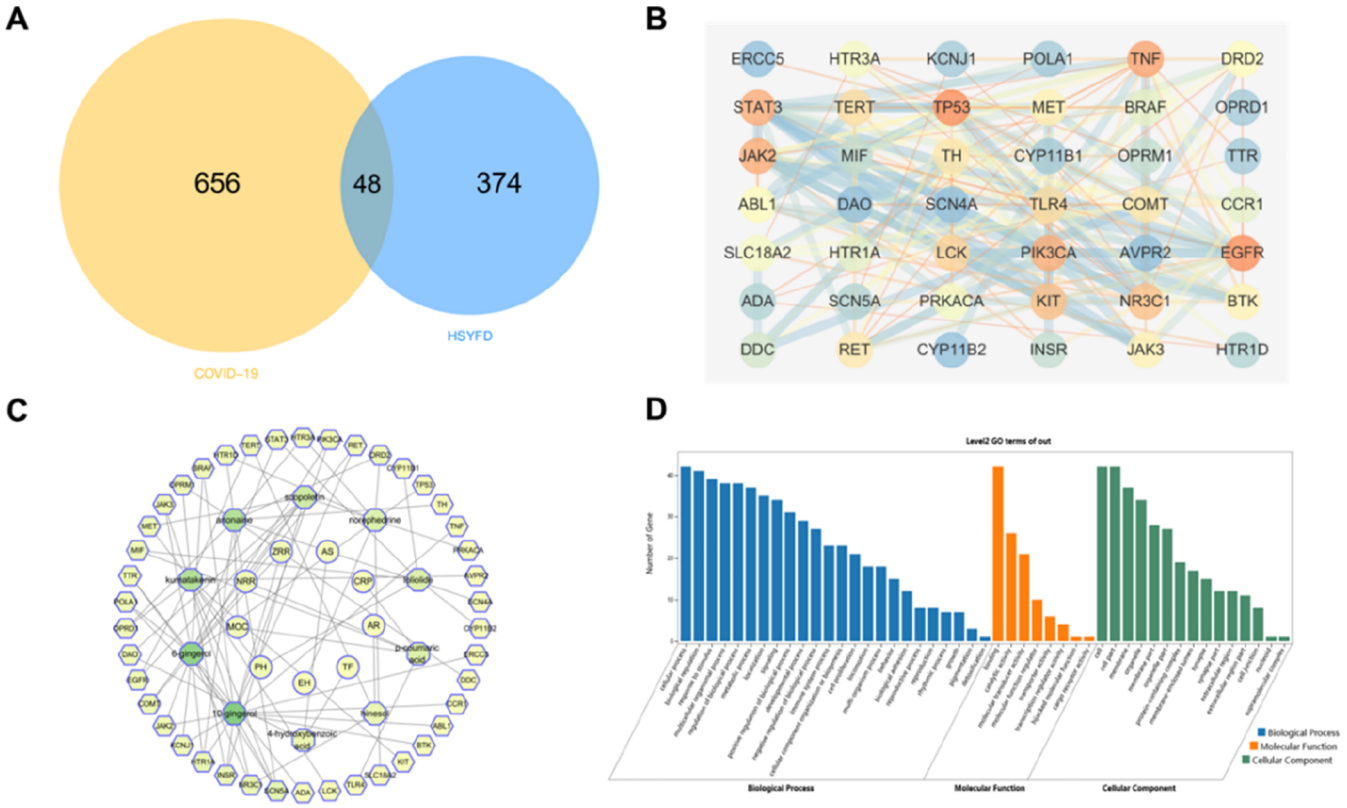

Figure 4. Therapeutic network of HSYFD. (A) Analysis of predicted active ingredients−disease target genes among herbs from HSYFD and COVID-19. (B) Protein−protein network of core target genes. (C) The herb−constituent−target network diagram of HSYFD in the treatment of COVID-19. The central circles represent the herbs, green represents the absorbed constituent, and the outer yellow circles represent the targets. (D) GO function analysis of targets of HSYFD against COVID-19. Blue represents the biological process, orange represents the molecular function, and green represents the cellular component.

adduct and isotopes 10 ppm was set in the criterion. After automatic identification, the MS FINDER 3.5.2 software, HMDB 5.0, and MassBank databases were used to confirm the characterized chemical components by checking the fragment structures. Detailed compound information is summarized in Table 1. A total of 108 chromatographic peaks were identified, of which 65 compositions were found in the positive mode, 37 compositions were detected in the negative mode, and 6 compositions were found in both the positive and negative modes.

The structural types of these compounds were mainly flavonoids, sesquiterpenoids, amino acids, and phenylpropanoids. Among the constituents, 9 compounds were from *AR*, 13 compounds were from *CRP*, 17 compounds were from MOC, 2 compounds were from *TF*, 12 compounds were from *EH*, 16 compounds were from NRR, 6 compounds were from ZRR, 12 compounds were from *AS*, and 8 compounds were from *PH*. 13 compounds were common compositions of multiple medicinal materials, such as both *AS* and *EH* contain ferulic acid.

2.3. Analysis of Prototype Constituents of HSYFD in Rat Serum. As 108 compounds were found from database 1.0, the retention times of those compounds were added in the library list, and therefore generated the three-dimensional data set (retention time-m/z-compounds) in Personal Compound Database Library (PCDL), which certainly was the database 2.0.[14−16] Normally, the method criterion for retention time was 0.25 min, and the average mass error of adduct and isotopes was 10 ppm. The rat serum was analyzed by the same UHPLC−Q-TOF-MS method, and therefore the absorbed prototype compounds were screened out by quick-matching the peaks in the database 2.0 using the Agilent MassHunter Qualitative Analysis 10.0 software.

Eleven chromatographic peaks were identified (Table 2, Figure 3). Among the constituents, hinesol was from *AR*, 10-gingerol and 6-gingerol were from ZRR, scopoletin was from NRR, anonaine was from *MOC*, loliolide and kumatakenin were from *PH*, norephedrine was from *EH*, histidine was from *AS*, *p*-coumaric acid was from MOC, CRP, and NRR, and 4-hydroxybenzoic acid was from *TF* and *AS*.

2.4. Network Pharmacology Analysis. *2.4.1. Potential Targets of the Active Ingredient of HSYFD.* A total of 422 putative targets of the 11 identified prototype constituents of HSYFD were obtained from the databases, and 704 potential targets were obtained by searching the genes related to Han-Shi-Yu-Fei symptoms of COVID-19 in the TCMIP V2.0. There were 48 overlapping targets from the compound-related targets and Han-Shi-Yu-Fei-related targets (Figure 4A). By constructing a protein−protein interaction (PPI) network for the abovementioned targets, it was found that a total of 42 targets interacted, forming a complex interlaced network. Among them, the betweenness centrality, closeness centrality, and degree of EGFR, TP53, TNF, JAK2, NR3C1, TH, COMT, and DRD2 were all higher than the average and were considered to be the core targets (Figure 4B, Table 3). To establish the relationship of herbs, compounds, and targets, we constructed a network of them. As shown in Figure 4C, the network consisted of 61 nodes and 84 edges, and the active

https://doi.org/10.1021/acsomega.2c04589
ACS Omega 2022, 7, 36598−36610

Table 3. Core Targets in the PPI Network

gene name	protein name	degree value	betweenness centrality	closeness centrality
EGFR	epidermal growth factor receptor	19	0.110916	0.569444
TP53	cellular tumor antigen p53	19	0.112516	0.525641
TNF	tumor necrosis factor	17	0.161021	0.539474
JAK2	tyrosine−protein kinase JAK2	16	0.057006	0.488095
NR3C1	glucocorticoid receptor	14	0.267501	0.569444
TH	tyrosine 3-monooxygenase	10	0.115960	0.506173
COMT	catechol O-methyltransferase	10	0.098256	0.427083
DRD2	D(2) dopamine receptor	8	0.041807	0.460674

ingredients of HSYFD correspond to multiple targets, and one target also corresponds to multiple active compounds; among them, 10-gingerol corresponds to 17 targets, 6-gingerol corresponds to 15 targets, both kumatakenin and anonaine correspond to 10 targets, they were the components with the most associated targets.

2.4.2. GO and KEGG Analyses of Potential Targets of the Active Ingredient of HSYFD. To probe the mechanisms of HSYFD in the treatment of mild stage of COVID-19, 42 targets were enriched by GO functional enrichment and KEGG pathway enrichment analyses. A total of 988 GO teams with a p-value < 0.001 were enriched, including 851 biological processes, 64 molecular functions, and 73 cellular components (Figure 4D). In detail, the biological process category mainly involved cellular process, biological regulation, and response to stimuli. Molecular function enrichment results primarily included binding, catalytic activity, and molecular transducer activity. In the cellular component category, targets were considered to be enriched in cell, cell part, and membrane. Multisteps were reported in the SARS-CoV-2 entry process. Specifically, in the steps that fusion between viral and cellular membranes, the viral RNA was released into the host cell cytoplasm for uncoating and replication.[17] GO analysis suggested that the therapeutic effect of HSYFD on COVID-19 may be attributed to its disruption of the interaction between viral and host cellular membranes.

Similarly, KEGG signaling pathways (P < 0.01) included multiple pathways that had been shown to be associated with COVID-19 (Table 4). For instance, both MAPK and PI3K/AKT signaling pathways contain multiple core targets (TNF, TP53, EGFR, and JAK2). It was reported that the MAPK pathway could regulate many cellular processes and were essential for immune cell function,[18] and the PI3K/AKT signaling pathway was associated with the activation of both CD147 and furin, which was also involved in the endocytosis of SARS-CoV-2.[19] Additionally, the process of virus invading cells was reported to cause changes in erbB, HIF-1, and mTOR pathways by the integrative proteo-transcriptomics analysis of Huh7 cells infected with SARS-CoV-2.[20] Moreover, SARS-CoV-2 could trigger inflammation through the JAK-STAT pathway, leading to the development of cytokine storms in cells such as lung cells and endothelial cells, causing lung injury.[21]

2.5. Molecular Docking Results. The binding activities of these core targets and the core compounds were preliminarily verified by molecular docking technology.[22] Results showed that the binding energies of almost all core targets to the molecules less than −5.0 kcal/mol (Figure 5). For example, the binding energies of COMT, JAK2, NR3C1, and TP53 to 6-gingerol were −5.8, −6.6, −6.7, and −5.8 kcal/mol, indicating that they displayed good binding activities, which was largely

Table 4. 20 Signaling Pathways Related to COVID-19

pathway	KEGG_class	genes	P value
MAPK signaling pathway	signal transduction	INSR, BRAF, KIT, TNF, MET, TP53, PRKACA, EGFR	0.000097200
Rap1 signaling pathway	signal transduction	INSR, DRD2, BRAF, KIT, MET, EGFR, PIK3CA	0.000102320
PI3K-Akt signaling pathway	signal transduction	INSR , TLR4, JAK2, KIT, JAK3, MET, TP53, EGFR, PIK3CA	0.000251609
HIF-1 signaling pathway	signal transduction	INSR, TLR4, EGFR, STAT3, PIK3CA	0.000296533
taste transduction	sensory system	HTR1A, PRKACA, HTR3A, HTR1D	0.000644398
cAMP signaling pathway	signal transduction	DRD2, BRAF, HTR1A, PRKACA, PIK3CA, HTR1D	0.000714311
ErbB signaling pathway	signal transduction	ABL1, BRAF, EGFR, PIK3CA	0.000880997
Necroptosis	cell growth and death	TLR4, JAK2, TNF, JAK3, STAT3	0.001287180
Jak-STAT signaling pathway	signal transduction	JAK2, JAK3, EGFR, STAT3, PIK3CA	0.001430151
neuroactive ligand−receptor interaction	signaling molecules and interaction	AVPR2 , DRD2, OPRM1, NR3C1, HTR1A, OPRD1, HTR1D	0.001489206
AGE-RAGE signaling pathway in diabetic complications	endocrine and metabolic diseases	JAK2, TNF, STAT3, PIK3CA	0.001583736
type II diabetes mellitus	endocrine and metabolic diseases	INSR, TNF, PIK3CA	0.001859059
Th17 cell differentiation	immune system	JAK2, JAK3, STAT3, LCK	0.002226016
insulin resistance	endocrine and metabolic diseases	INSR, TNF, STAT3, PIK3CA	0.002298795
sphingolipid signaling pathway	signal transduction	TNF, TP53, PIK3CA, OPRD1	0.003210978
phenylalanine metabolism	amino acid metabolism	DDC, MIF	0.003455026
inflammatory bowel disease (IBD)	immune diseases	TLR4, TNF, STAT3	0.004849935
insulin signaling pathway	endocrine system	INSR, BRAF, PRKACA, PIK3CA	0.005453038
Parkinson disease	neurodegenerative diseases	SLC18A2, DRD2, TH, PRKACA	0.006891435
mTOR signaling pathway	signal transduction	INSR, BRAF, TNF, PIK3CA	0.008208998

https://doi.org/10.1021/acsomega.2c04589
ACS Omega 2022, 7, 36598−36610

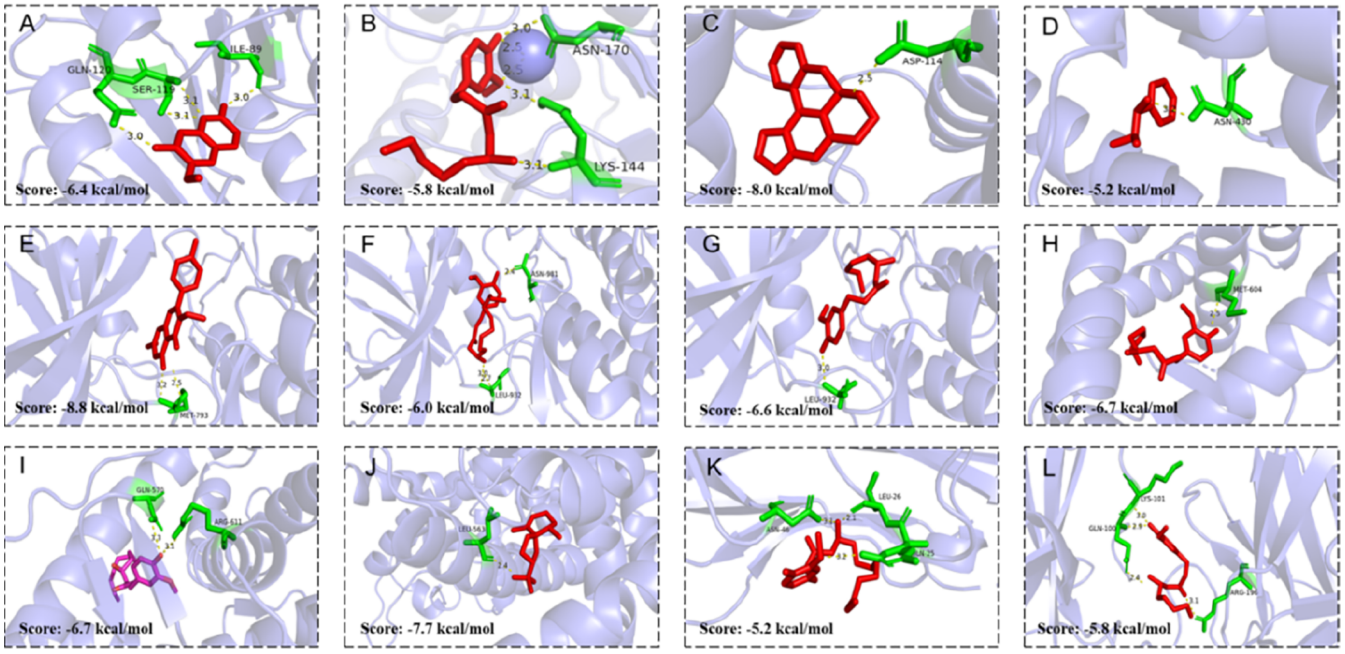

Figure 5. Molecular docking results. (A) COMT with scopoletin; (B) COMT with 6-gingerol; (C) DRD2 with anonaine; (D) DRD2 with norephedrine; (E) EGFR with kumatakenin; (F) JAK2 with 10-gingerol; (G) JAK2 with 6-gingerol; (H) NR3C1 with 6-gingerol; (I) NR3C1 with 10-gingerol; (J) NR3C1 with hinesol; (K) TNF with 10-gingerol; (L) TP53 with 6-gingerol.

consistent with the previous compound-target result by network pharmacology analysis.

3. DISCUSSION

For orally administrated TCM recipe, systematic identification of the blood-absorbing compounds is critical to understanding its pharmacodynamic material basis and the therapeutic mechanism.[23] Therefore, first, a total of 108 components were identified from HSYFD by the UHPLC−Q-TOF-MS technique. The qualitative analysis characterization compounds mainly consisted of flavonoids, sesquiterpenoids, amino acids, and phenylpropanoids. Next, a total of 11 prototype components were identified from the rat serum after oral administration of HSYFD, which could be recognized as the potential material basis for the efficacy of HSYFD. In particular, kumatakenin from PH showed good inhibitory activity against SARS-CoV-2 replication in Vero E6 and Calu-3 cells, whose inhibitory effects were even better than those of lopinavir/ritonavir and chloroquine.[24] In addition, 10-gingerol and 6-gingerol, two key compounds based on degree ranking in herb−constituent−target network analysis, showed anti-inflammatory, immune regulation, and anti-nausea activities.[25] In some situations, the elevated inflammatory markers were also identified as risk factors for psychoticism symptoms, which could induce depression in COVID-19 patients.[26,27] Moreover, scopoletin from NRR promotes glutamatergic modulating effects and could regulate depression by increasing synaptic plasticity in prefrontal regions.[28]

Although COVID-19 was diagnosed based on reverse transcription polymerase chain reaction, the patients were classified as mild, moderate, severe, or critical depending on the clinical severity of their prominent clinical symptoms. In the initial viral phase, about 80% of patients usually have mild or asymptomatic disease. In the second phase, host−virus interactions take place which dictate the outcome for the subsequent phases of the disease, which corresponded to a hyper-responsiveness of the immune system. Given this characterization, the typical clinical manifestations were the representatives of the targets of COVID-19. Thus, it is worth noting that the disease targets were obtained by the clinical symptom-guided searching, and, interestingly, the commonly used known related targets for COVID-19 such as NR3C1,[29] JAK2,[30] JAK3,[31] MIF,[32] and STAT3[33] had been overlapped.

KEGG analysis revealed many pathways associated with COVID-19, such as MAPK signaling pathway, PI3K/AKT signaling pathway, and JAK-STAT pathway. The PPI network found that EGFR, TP53, TNF, JAK2, NR3C1, TH, COMT, and DRD2 were the core targets of HSYFD in the treatment of COVID-19. The role of inflammatory mechanism had been highlighted in the pathogenesis of COVID-19. Tumor necrosis factor (TNF), another key mediator of triggering the cytokine storm, showed high levels in organs such as the lymph nodes of COVID-19 patients, which could prevent the body from producing memory B cells, thereby inhibiting the generation of a durable immune response.[34] At present, the JAK inhibitor baricitinib, which could reduce inflammation by inhibiting the levels of cytokines such as IL-6, IL-1β, and TNF-α and regulate the immune environment, was approved by FDA for the treatment of hospitalized adult patients with COVID-19.[35] According to the COVID-19 pathological characteristics, the overexpressed EGFR in the infected lung cells exacerbates pulmonary fibrosis as the severe consequence of cytokine storm, evidenced by the transcriptomic data of patients.[36] Additionally, the lung lesions in COVID-19 patients could be alleviated by the treatment of anti-EGFR antibodies like nimotuzumab, accompanied with the reduced plasma IL-6 level.[37] In addition, protective and immunomodulatory effects of TCM were observed by augmenting TNF-α and IL-6 expression in the animal model of acute lung inflammation. Recent accumulating data suggested that TP53 gene therapy may be a new treatment for COVID-19 patients,[38] and it was therefore concluded that the compounds from HSYFD might

https://doi.org/10.1021/acsomega.2c04589
ACS Omega 2022, 7, 36598−36610

augment TP53 expression. For example, 6-gingerol, which showed good binding activities to TP53, could promote the activation of TP53.[39]

The subsequent molecular docking computational analysis confirmed the constituent−target interactions from the network pharmacology results. Based on the description above, it was speculated that HSYFD may play a role in the treatment of COVID-19 via MAPK signaling pathway, PI3K/AKT signaling pathway, and JAK-STAT pathway.

Although 108 compounds were identified for HSYFD, only 11 prototype compounds as the absorbed constituents were characterized in the rat serum. However, those unabsorbed constituents were not considered key active constituents because of the multiple complex ingredient−body interactions. Sometimes, unabsorbed compounds such as flavonoids were metabolized by the gut microbiota to smaller metabolites, which were more bioavailable than their precursors.[40] Moreover, microbiological studies showed that unabsorbed components could prompt the growth of beneficial bacteria and inhibit the growth of disease-causing bacteria, contributing to maintain the homeostasis of the digestive system and gut flora.[41] Of course, the alterations of gut microbiota in COVID-19 patients consequently may lead to the development of gut dysbiosis-related diseases. Therefore, it was also recommended for the recovery of gut microbiota balance while treating COVID-19 patients.[42] Many Chinese herbs and preparations have demonstrated properties of restoring intestinal barrier function and intestinal homeostasis, which may further modulate the immune function after SARS-CoV-2 infection.[43,44] Understanding the role of compounds in maintaining intestinal flora balance could provide new ideas for preventing and treating COVID-19.

At present, FDA-approved anti-SARS-CoV-2 drugs such as Paxlovid, Molnupiravir, and remdesivir, mainly focus only on individual targets like 3CL protease and RdRp, and it took plenty of time and capital to discover the new drug, which is still effective on the front of continuous mutation of SARS-CoV-2.[45−47] Based on a specific theory, numerous clinical data evidenced the TCM for many known infectious disease treatments. More importantly, TCM played an irreplaceable role in the prevention and treatment of unknown COVID-19 since its first epidemic, especially in the treatment of mild patients.[48,49] Furthermore, current clinical trials are devoted to finding the superiority of the combination of the TCM and western medicine in the treatment of COVID-19 patients infected with Delta or Omicron variants, when compared with the western medicine treatment.[50]

4. CONCLUSIONS

In this work, the chemical components of HSYFD in vivo and in vitro were analyzed by a UHPLC−Q-TOF-MS method, and the mechanism for treating COVID-19 was explored by clinical symptom-guided network pharmacology technology with molecular docking. A total of 108 components were identified from HSYFD, of which 11 components were detected in the rat serum after its oral administration. MAPK signaling pathway, PI3K/AKT signaling pathway, and JAK-STAT pathway were recognized as the key pathways of HSYFD for confronting COVID-19, with COMT, DRD2, EGFR, JAK2, NR3C1, TNF, and TP53 as the key targets. Our work also verified the feasibility of clinical symptom-guided network pharmacology analysis for the chemical compounds, which provided a possible agreement between the points of view of TCM and western medicine on the disease.

5. MATERIALS AND METHODS

5.1. Materials and Reagents. AR (19091207, Inner Mongolia), CRP (19090603, Zhejiang Province), MOC (19042803, Fujian Province), PH (19051410, Zhejiang Province), TF (18032901, Yunnan Province), EH (15092512, Shanxi Province), NRR (19011512, Qinghai Province), AS (19010309, Guangdong Province), and ZRR (20200308, Shanghai Province) were purchased from Wujiang District Shanghai Cai Tong de Tang Chinese herbal pieces Co., Ltd., and identified by Prof. Chen Wan-sheng from Shanghai University of Traditional Chinese Medicine. Hesperidin (P06D9F77001), 6-shogaol (P06N9L74388), and notopterol (R28m9f57295) were purchased from Shanghai Yuanye Biotechnology Co., Ltd. (purity ≥ 98%). Ultra-pure water was prepared using a Milli-Q water purification system (Bedford, France). Acetonitrile and methanol were of UPLC grade (Merck, Darmstadt, Germany). All other reagents were of analytical grade.

5.2. Preparation of the HSYFD Extract. AR (105 g), CRP (70 g), MOC (70 g), PH (70 g), TF (42 g), EH (42 g), NRR (70 g), ZRR(70 g), and AS (70 g) were co-decocted in water twice, for 1 h each time. Water added in the first round was 10 times the total weight of the herbs, and in the second round it was 8 times the total weight of the herbs. The extraction solutions were then filtered, combined, and concentrated under vacuum to yield 610 mL of a concentrated decoction (HSYFD, 0.998 g/mL). About 10 mL of the HSYFD was centrifuged at 3000 r/min for 10 min, transferred into a 1.5 mL centrifuge tube, and centrifuged again at 13,000 rpm for 15 min. 200 μL of the supernatant was then subjected to UHPLC−Q-TOF-MS analysis. The remaining decoction was freeze-dried to obtain lyophilized powder, dissolved in normal saline by ultrasound to form a solution equivalent to a crude drug concentration of 7 g/mL, and stored at 4 °C before intragastric administration.

5.3. UHPLC−Q-TOF-MS Analysis. An Agilent 1290 ultra-performance liquid chromatography system (Agilent Technologies, Santa Clara, California, USA) coupled with an Agilent 6530 Accurate Quality Q-TOF/MS system (Agilent Technologies, USA) was employed in this study. Chromatographic separation was performed on a Waters Acquity UPLC BEH C18 column (2.1 × 100 mm, 1.7 μm). The mobile phase consisted of 0.1% formic acid−water (phase A) and acetonitrile (phase B). The gradient elution procedure was set as follows: 0−3 min, 5−5% B; 3−15 min, 5−35% B; 15−29 min, 35−95% B; 29−30 min, 95% B. The flow rate was 0.3 mL/min. The column temperature was maintained at 30 °C. The injection volume was 1 μL for the HSYFD sample and 2 μL for the serum. The UV spectra were recorded at 254 and 360 nm.

Parameters for Electrospray Mass Spectrometry (ESI-MS) analysis were set as follows: scan range, mass-to-charge ratio (m/z), 100−1700; dry gas (N_2) temperature, 350 °C; dry gas flow, 11.0 L/min; atomizer gas pressure, 45 psi; capillary voltage, 4000 V (positive)/3500 V (negative); divider voltage, 140 V; collision energy, 30 V. All data were obtained with reference masses at m/z 121.0509 and 922.0098 in the positive mode, and at m/z 1033.9881 in the negative mode. QC samples were injected after every five samples during the sequence analysis to evaluate the analytical performance.

https://doi.org/10.1021/acsomega.2c04589
ACS Omega 2022, 7, 36598−36610

Agilent mass Hunter qualitative analysis B.10.00 was used for data collection and processing. MS finder 3.5.0 (http://prime.psc.riken.jp/compms/msfinder/main.html), HMDB 5.0 (https://hmdb.ca/), and Massbank (http://www.massbank.jp/) were used to further confirm the compound information.

5.4. Animals and Drug Administration. Twelve SPF grade male Sprague−Dawley rats (220 ± 20 g) were obtained from the Shanghai Institute of Planned Parenthood Research (Shanghai, China) and were housed in accordance with the Animal Ethics Committee of Shanghai University of Traditional Chinese Medicine (PZSHUTCM201113012). All rats were stored in a room with controlled temperature (22−26 °C) and humidity (40−70%), under a 12 h light−dark cycle. Animals were acclimatized to the facility for 1 week before the start of the experiment. Rats were randomly divided into two groups (n = 6 for each group) before the experiment. Rats in the HSYFD group were dosed at 70 g crude drug/kg/day for three consecutive days, while 0.9% normal saline (2 mL/day) was administered to the rats in the control group.

5.5. Serum Sample Collection and Pretreatment Method. Blood samples were collected from the infraorbital vein 1 h after the last administration of HSYFD and stored in 5 mL BD Vacutainer Plus Plastic Blood Collection Tubes. Serum was obtained by centrifugation at 3000 rpm at 4 °C for 10 min after standing for 2 h at room temperature (25 °C), and 100 μL of which was deproteinized with 400 μL of ice-cold methanol. After being vortexed for 1 min and centrifuged at 4 °C at 12,000 rpm for 15 min, the supernatant was transferred to a new centrifuge tube, lyophilized, and then reconstituted in 100 μL of methanol. The supernatant was centrifuged at 12,000 rpm for 10 min at 4 °C, and the supernatant was prepared for UHPLC−Q-TOF-MS analysis.

5.6. Target Network Analysis. The potential targets of the compounds were obtained from Swiss Target Prediction (http://www.swisstargetprediction.ch) and TCMSP (https://tcmspw.com/tcmsp.php). Based on TCMIP V2.0 (http://www.tcmip.cn), the HSYF phenotype targets were obtained by retrieving the entries of clinical symptom of mild stage of COVID-19, including fever, cough, abnormality of the pharynx, fatigue, anergy, dyspnea, abnormality of the stomach, nausea, vomiting, diarrhea, abnormality of the tongue, and abnormality of the vasculature.

The ImageGP website (http://www.ehbio.com/ImageGP/) was used to identify the common targets of HSYFD and COVID-19. The OmicShare cloud platform (https://www.omicshare.com/tools/) was used for dynamic GO enrichment analysis and KEGG pathway enrichment analysis of the abovementioned common targets, and "homo sapiens" was selected as the gene source. Significance was set at $P < 0.001$ for GO entries and at $P < 0.01$ for signal pathways. The common targets were also used to construct a PPI network model on the String website, and then input into Cytoscape 3.7.2 to obtain the PPI network, and the network analyzer function in the software was used to obtain the relevant network topology parameters. The core targets of HSYFD treatment of COVID-19 were screened with the three indices of degree of degrees, betweenness centrality, and closeness centrality, all of which exceeded the average values.[51]

5.7. Molecular Docking Analysis. The 3D structures of the core targets were obtained from the PDB database (http://www.rcsb.org) and AlphaFold (https://alphafold.ebi.ac.uk). PyMOL software was used to remove excess water molecules and inactive ligands. 3D structures of the compound corresponding to the core target from PubChem were converted to PDB format by openbabel 3.1.1 and saved as pdbqt format using autodock tools 1.5.7. Autodock Vina and PyMOL software were used for molecular docking and visualization.[52]

AUTHOR INFORMATION

Corresponding Authors

Feng Zhang − *Department of Pharmacy, Changzheng Hospital, (Second Military Medical University), Naval Medical University, Shanghai 200003, China; Shanghai Key Laboratory for Pharmaceutical Metabolite Research, Shanghai 200433, China; Department of Pharmacology, Anhui University of Chinese Medicine, Hefei 230012 Anhui, China*; Email: fengzhang@smmu.edu.cn

Wansheng Chen − *Institute of Chinese Materia Medica, Shanghai University of Traditional Chinese Medicine, Shanghai 201203, China; Department of Pharmacy, Changzheng Hospital, (Second Military Medical University), Naval Medical University, Shanghai 200003, China; Shanghai Key Laboratory for Pharmaceutical Metabolite Research, Shanghai 200433, China*; orcid.org/0000-0002-0025-1315; Email: chenwansheng@smmu.edu.cn

Authors

Guangyang Jiao − *Institute of Chinese Materia Medica, Shanghai University of Traditional Chinese Medicine, Shanghai 201203, China*; orcid.org/0000-0001-5486-032X

Xiangcheng Fan − *Department of Pharmacy, Changzheng Hospital, (Second Military Medical University), Naval Medical University, Shanghai 200003, China; Shanghai Key Laboratory for Pharmaceutical Metabolite Research, Shanghai 200433, China*; orcid.org/0000-0001-9563-9701

Yejian Wang − *Department of Pharmacology, Anhui University of Chinese Medicine, Hefei 230012 Anhui, China*

Nan Weng − *Department of Pharmacy, Changzheng Hospital, (Second Military Medical University), Naval Medical University, Shanghai 200003, China; School of Traditional Chinese Material, Shenyang Pharmaceutical University, Shenyang 11001, China*

Luolan Ouyang − *School of Pharmacy, Shanghai University of Chinese Medicine, Shanghai 201203, China*

Haoqian Wang − *School of Pharmacy, Shanghai University of Chinese Medicine, Shanghai 201203, China*

Sihan Pan − *School of Pharmacy, Shanghai University of Chinese Medicine, Shanghai 201203, China*

Doudou Huang − *Institute of Chinese Materia Medica, Shanghai University of Traditional Chinese Medicine, Shanghai 201203, China*

Jun Han − *Department of Gastroenterology, Changzheng Hospital, (Second Military Medical University), Naval Medical University, Shanghai 200003, China*

Complete contact information is available at: https://pubs.acs.org/10.1021/acsomega.2c04589

Author Contributions

G.-Y.J. and X.-C.F. contributed equally to this study and were co-first authors. Manuscript writing, G.-Y.J. and X.-C.F.; manuscript revision and data checking, F.Z. and D.-D.H.; rat experimental, G.-Y.J. and X.-C.F.; UHPLC−Q-TOF-MS analysis, G.-Y.J., Y.-J.W., N.W., and L.-L.O.Y.; network

https://doi.org/10.1021/acsomega.2c04589
ACS Omega 2022, 7, 36598−36610

pharmacology, G.-Y.J., H.-Q.W., and S.-H. P.; project administration, W.-S.C.; funding acquisition, F.Z. and W.-S.C. All authors have read and approved the final version of the manuscript.

Notes

The authors declare no competing financial interest.

The animal study was reviewed and approved by the Animal Ethics Committee of Shanghai University of Traditional Chinese Medicine (PZSHUTCM201113012).

The raw data sets used and analyzed during the study are available on request to the senior author (W.-S.C., chenwansheng@smmu.edu.cn).

■ ACKNOWLEDGMENTS

This project was supported by the National Natural Science Foundation of China (81830109), Jin-Zi-Ta Talent projects (0806 and 1016), and Innovative Clinical Research Funding Project (2020YLCYJ-Y25).

■ REFERENCES

(1) Telenti, A.; Arvin, A.; Corey, L.; Corti, D.; Diamond, M. S.; García-Sastre, A.; Garry, R. F.; Holmes, E. C.; Pang, P. S.; Virgin, H. W. After the pandemic: perspectives on the future trajectory of COVID-19. *Nature* **2021**, *596*, 495−504.

(2) Song, B. Correlation Between the Periodization of Traditional Chinese Medicine and the Classification of Western Medicine in the Diagnosis and Treatment for Novel Coronavirus Pneumonia (Trial Version Fifth). *J. Tradit. Chin. Med.* **2020**, *61*, 1200−1203.

(3) Ming, L.; Fan, G.; Xiao, G.; Wang, T.; Xu, D.; Gao, J.; Ge, S.; Li, Q.; Ma, Y.; Zhang, H.; Wang, J.; Cui, Y.; Zhang, J.; Zhu, Y.; Zhang, B. Traditional Chinese medicine in COVID-19. *Acta Pharm. Sin. B* **2021**, *11*, 3337−3363.

(4) Wu, C.; Chen, X.; Cai, Y.; Xia, J.; Zhou, X.; Xu, S.; Huang, H.; Zhang, L.; Zhou, X.; Du, C.; Zhang, Y.; Song, J.; Wang, S.; Chao, Y.; Yang, Z.; Xu, J.; Zhou, X.; Chen, D.; Xiong, W.; Xu, L.; Zhou, F.; Jiang, J.; Bai, C.; Zheng, J.; Song, Y. Risk Factors Associated With Acute Respiratory Distress Syndrome and Death in Patients With Coronavirus Disease 2019 Pneumonia in Wuhan, China. *JAMA Intern. Med.* **2020**, *180*, 934−943.

(5) Rodríguez, Y.; Novelli, L.; Rojas, M.; DeSantis, M.; Acosta-Ampudia, Y.; Monsalve, D. M.; Ramírez-Santana, C.; Costanzo, A.; Ridgway, W. M.; Ansari, A. A.; Gershwin, M. E.; Selmi, C.; Anaya, J. M. Autoinflammatory and autoimmune conditions at the crossroad of COVID-19. *J. Autoimmun.* **2020**, *114*, 102506.

(6) Xu, H.-Y.; Zhang, Y.-Q.; Qin, Y.-F.; Zhao, H.-Y.; Wang, P.; Liu, F. Exploration on scientific connotation of TCM syndromes and recommended prescriptions against COVID-19 based on TCMTP V2. 0. *Zhongguo Zhongyao Zazh* **2020**, *45*, 1488−1498.

(7) Leung, E. L. H.; Pan, H. D.; Huang, Y. F.; Fan, X. X.; Wang, W. Y.; He, F.; Cai, J.; Zhou, H.; Liu, L. The Scientific Foundation of Chinese Herbal Medicine against COVID-19. *Engineering* **2020**, *6*, 1099−1107.

(8) Li, L.; Wu, Y.; Wang, J.; Yan, H. M.; Lu, J.; Wang, Y.; Zhang, B. L.; Zhang, J. H.; Yang, J.; Wang, X. Y.; Zhang, M.; Li, Y.; Miao, L.; Zhang, H. Potential Treatment of COVID-19 with Traditional Chinese Medicine: What Herbs Can Help Win the Battle with SARS-CoV-2? *Engineering* **2021**, DOI: 10.1016/j.eng.2021.08.020.

(9) Kang, X. M.; Jin, D.; Jiang, L. L.; Zhang, Y. Q.; Zhang, Y. H.; An, X. D.; Duan, L. Y.; Yang, C. Q.; Zhou, R. Q.; Duan, Y. Y.; Sun, Y. T.; Lian, F. M. Efficacy and mechanisms of traditional Chinese medicine for COVID-19: a systematic review. *Chin. Med.* **2022**, *17*, 30.

(10) Kong, X.; Liu, C.; Lu, P.; Guo, Y.; Zhao, C.; Yang, Y.; Bo, Z.; Wang, F.; Peng, Y.; Meng, J. Combination of UPLC-Q-TOF/MS and Network Pharmacology to Reveal the Mechanism of Qizhen Decoction in the Treatment of Colon Cancer. *ACS Omega* **2021**, *6*, 14341−14360.

(11) Zhang, F.; Li, Z.; Li, M.; Yuan, Y.; Cui, S.; Chen, J.; Li, R. Dissection of the potential anti-influenza materials and mechanism of Lonicerae japonicae flos based on in vivo substances profiling and network pharmacology. *J. Pharm. Biomed. Anal.* **2021**, *193*, 113721.

(12) Li, N.; Xie, L.; Yang, N.; Sun, G.; Liu, H.; Bi, C.; Duan, J.; Yuan, Y.; Yu, H.; Xu, Y.; Li, Y. Rapid classification and identification of chemical constituents in Epimedium koreanum Nakai by UPLC-Q-TOF-MS combined with data post-processing techniques. *Phytochem. Anal.* **2021**, *32*, 575−591.

(13) Yang, N.; Dong, Y.; Wu, M.; Li, S.; Yu, H.; Yang, S. Establishing a rapid classification and identification method for the major triterpenoids of Alisma orientale. *Phytochem. Anal.* **2020**, *31*, 384−394.

(14) Zhu, Z. J.; Schultz, A. W.; Wang, J.; Johnson, C. H.; Yannone, S. M.; Patti, G. J.; Siuzdak, G. Liquid chromatography quadrupole time-of-flight mass spectrometry characterization of metabolites guided by the METLIN database. *Nat. Protoc.* **2013**, *8*, 451−460.

(15) Marin, S. J.; Hughes, J. M.; Lawlor, B. G.; Clark, C. J.; McMillin, G. A. Rapid screening for 67 drugs and metabolites in serum or plasma by accurate-mass LC-TOF-MS. *J. Anal. Toxicol.* **2012**, *36*, 477−486.

(16) Turova, P.; Rodin, I.; Shpigun, O.; Stavrianidi, A. A new PARAFAC-based algorithm for HPLC-MS data treatment: herbal extracts identification. *Phytochem. Anal.* **2020**, *31*, 948−956.

(17) Jackson, C. B.; Farzan, M.; Chen, B.; Choe, H. Mechanisms of SARS-CoV-2 entry into cells. *Nat. Rev. Mol. Cell Biol.* **2022**, *23*, 3−20.

(18) Goel, S.; Saheb Sharif-Askari, F.; Saheb Sharif Askari, N.; Madkhana, B.; Alwaa, A. M.; Mahboub, B.; Zakeri, A. M.; Ratemi, E.; Hamoudi, R.; Hamid, Q.; Halwani, R. SARS-CoV-2 Switches "on" MAPK and NFκB Signaling via the Reduction of Nuclear DUSP1 and DUSP5 Expression. *Front. Pharmacol.* **2021**, *12*, 631879.

(19) Khezri, M. R. PI3K/AKT signaling pathway: a possible target for adjuvant therapy in COVID-19. *Hum. Cell* **2021**, *34*, 700−701.

(20) Appelberg, S.; Gupta, S.; Svensson Akusjärvi, S.; Ambikan, A. T.; Mikaeloff, F.; Saccon, E.; Végvári, Á.; Benfeitas, R.; Sperk, M.; Ståhlberg, M.; Krishnan, S.; Singh, K.; Penninger, J. M.; Mirazimi, A.; Neogi, U. Dysregulation in Akt/mTOR/HIF-1 signaling identified by proteo-transcriptomics of SARS-CoV-2 infected cells. *Emerg. Microb. Infect.* **2020**, *9*, 1748−1760.

(21) Luo, W.; Li, Y.; Jiang, L.; Chen, Q.; Wang, T.; Ye, D. Targeting JAK-STAT Signaling to Control Cytokine Release Syndrome in COVID-19. *Trends Pharmacol. Sci.* **2020**, *41*, 531−543.

(22) Song, X.; Zhang, Y.; Dai, E.; Wang, L.; Du, H. Prediction of triptolide targets in rheumatoid arthritis using network pharmacology and molecular docking. *Int. Immunopharmacol.* **2020**, *80*, 106179.

(23) Xu, H. Y.; Zhang, Y. Q.; Wang, P.; Zhang, J. H.; Chen, H.; Zhang, L. Q.; Du, X.; Zhao, C. H.; Wu, D.; Liu, F.; Yang, H. J.; Liu, C. X. A comprehensive review of integrative pharmacology-based investigation: A paradigm shift in traditional Chinese medicine. *Acta Pharm. Sin. B* **2021**, *11*, 1379−1399.

(24) Leal, C. M.; Leitão, S. G.; Sausset, R.; Mendonça, S. C.; Nascimento, P. H. A.; de Araujo R. Cheohen, C. F.; Esteves, M. E. A.; Leal da Silva, M.; Gondim, T. S.; Monteiro, M. E. S.; Tucci, A. R.; Fintelman-Rodrigues, N.; Siqueira, M. M.; Miranda, M. D.; Costa, F. N.; Simas, R. C.; Leitão, G. G. Flavonoids from Siparuna cristata as Potential Inhibitors of SARS-CoV-2 Replication. *Rev. Bras. Farmacogn.* **2021**, *31*, 658−666.

(25) Semwal, R. B.; Semwal, D. K.; Combrinck, S.; Viljoen, A. M. Gingerols and shogaols: Important nutraceutical principles from ginger. *Phytochemistry* **2015**, *117*, 554−568.

(26) Papava, I.; Dehelean, L.; Romosan, R. S.; Bondrescu, M.; Dimeny, C. Z.; Domuta, E. M.; Bratosin, F.; Bogdan, I.; Grigoras, M. L.; Tigmeanu, C. V.; Gherman, A.; Marincu, I. The Impact of Hyper-Acute Inflammatory Response on Stress Adaptation and Psychological Symptoms of COVID-19 Patients. *Int. J. Environ. Res. Publ. Health* **2022**, *19*, 6501.

(27) Mazza, M. G.; De Lorenzo, R.; Conte, C.; Poletti, S.; Vai, B.; Bollettini, I.; Melloni, E.; Furlan, R.; Ciceri, F.; Rovere-Querini, P.; Benedetti, F. Anxiety and depression in COVID-19 survivors: Role of

https://doi.org/10.1021/acsomega.2c04589
ACS Omega 2022, 7, 36598−36610

inflammatory and clinical predictors. *Brain Behav. Immun.* **2020**, *89*, 594−600.
(28) Tarai, S.; Mukherjee, R.; Gupta, S.; Rizvanov, A. A.; Palotás, A.; Chandrasekhar Pammi, V. S.; Bit, A. Influence of pharmacological and epigenetic factors to suppress neurotrophic factors and enhance neural plasticity in stress and mood disorders. *Cogn Neurodyn* **2019**, *13*, 219−237.
(29) Basar, R.; Uprety, N.; Ensley, E.; Daher, M.; Klein, K.; Martinez, F.; Aung, F.; Shanley, M.; Hu, B.; Gokdemir, E.; Nunez Cortes, A. K.; Mendt, M.; Reyes Silva, F.; Acharya, S.; Laskowski, T.; Muniz-Feliciano, L.; Banerjee, P. P.; Li, Y.; Li, S.; Melo Garcia, L.; Lin, P.; Shaim, H.; Yates, S. G.; Marin, D.; Kaur, I.; Rao, S.; Mak, D.; Lin, A.; Miao, Q.; Dou, J.; Chen, K.; Champlin, R. E.; Shpall, E. J.; Rezvani, K. Generation of glucocorticoid-resistant SARS-CoV-2 T cells for adoptive cell therapy. *Cell Rep.* **2021**, *36*, 109432.
(30) Wu, D.; Yang, X. O. TH17 responses in cytokine storm of COVID-19: An emerging target of JAK2 inhibitor Fedratinib. *J. Microbiol. Immunol. Infect.* **2020**, *53*, 368−370.
(31) Levy, G.; Guglielmelli, P.; Langmuir, P.; Constantinescu, S. JAK inhibitors and COVID-19. *J. Immunother. Cancer.* **2022**, *10*, No. e002838.
(32) Kovarik, J. J.; Kämpf, A. K.; Gasser, F.; Herdina, A. N.; Breuer, M.; Kaltenecker, C. C.; Wahrmann, M.; Haindl, S.; Mayer, F.; Traby, L.; Touzeau-Roemer, V.; Grabmeier-Pfistershammer, K.; Kussmann, M.; Robak, O.; Willschke, H.; Ay, C.; Säemann, M. D.; Schmetterer, K. G.; Strassl, R. Identification of Immune Activation Markers in the Early Onset of COVID-19 Infection. *Front. Cell. Infect. Microbiol.* **2021**, *11*, 651484.
(33) Gajjela, B. K.; Zhou, M. Calming the cytokine storm of COVID-19 through inhibition of JAK2/STAT3 signaling. *Drug Discov. Today* **2022**, *27*, 390−400.
(34) Kaneko, N.; Kuo, H.; Boucau, J.; Farmer, J. R.; Allard-Chamard, H.; Mahajan, V. S.; Piechocka-Trocha, A.; Lefteri, K.; Osborn, M.; Bals, J.; Bartsch, Y. C.; Bonheur, N.; Caradonna, T. M.; Chevalier, J.; Chowdhury, F.; Diefenbach, T. J.; Einkauf, K.; Fallon, J.; Feldman, J.; Finn, K. K.; Garcia-Broncano, P.; Hartana, C. A.; Hauser, B. M.; Jiang, C.; Kaplonek, P.; Karpell, M.; Koscher, E. C.; Lian, X.; Liu, H.; Liu, J.; Ly, N. L.; Michell, A. R.; Rassadkina, Y.; Seiger, K.; Sessa, L.; Shin, S.; Singh, N.; Sun, W.; Sun, X.; Ticheli, H. J.; Waring, M. T.; Zhu, A. L.; Alter, G.; Li, J. Z.; Lingwood, D.; Schmidt, A. G.; Lichterfeld, M.; Walker, B. D.; Yu, X. G.; Padera, R. F. J.; Pillai, S. Loss of Bcl-6-Expressing T Follicular Helper Cells and Germinal Centers in COVID-19. *Cell* **2020**, *183*, 143−157.
(35) Bronte, V.; Ugel, S.; Tinazzi, E.; Vella, A.; De Sanctis, F.; Canè, S.; Batani, V.; Trovato, R.; Fiore, A.; Petrova, V.; Hofer, F.; Barouni, R. M.; Musiu, C.; Caligola, S.; Pinton, L.; Torroni, L.; Polati, E.; Donadello, K.; Friso, S.; Pizzolo, F.; Iezzi, M.; Facciotti, F.; Pelicci, P. G.; Righetti, D.; Bazzoni, P.; Rampudda, M.; Comel, A.; Mosaner, W.; Lunardi, C.; Olivieri, O. Baricitinib restrains the immune dysregulation in patients with severe COVID-19. *J. Clin. Invest.* **2020**, *130*, 6409−6416.
(36) Vagapova, E. R.; Lebedev, T. D.; Prassolov, V. S. Viral fibrotic scoring and drug screen based on MAPK activity uncovers EGFR as a key regulator of COVID-19 fibrosis. *Sci. Rep.* **2021**, *11*, 11234.
(37) Abdo Cuza, A. A.; Pi Ávila, J.; Machado Martínez, R.; Jordán González, J.; Pérez Aspuro, G.; Gutiérrez Martínez, J. A.; Ramos Suzarte, M.; Saavedra Hernández, D.; Añé-Kouri, A. L.; Crombet Ramos, T. Nimotuzumab for COVID-19: case series. *Immunotherapy* **2022**, *14*, 185−193.
(38) Harford, J. B.; Kim, S. S.; Pirollo, K. F.; Chang, E. H. TP53 Gene Therapy as a Potential Treatment for Patients with COVID-19. *Viruses* **2022**, *14*, 739−752.
(39) Wala, K.; Szlasa, W.; Sauer, N.; Kasperkiewicz-Wasilewska, P.; Szewczyk, A.; Saczko, J.; Rembiałkowska, N.; Kulbacka, J.; Baczyńska, D. Anticancer Efficacy of 6-Gingerol with Paclitaxel against Wild Type of Human Breast Adenocarcinoma. *Molecules* **2022**, *27*, 2693.
(40) Bitner, B. F.; Ray, J. D.; Kener, K. B.; Herring, J. A.; Tueller, J. A.; Johnson, D. K.; Tellez Freitas, C. M.; Fausnacht, D. W.; Allen, M. E.; Thomson, A. H.; Weber, K. S.; McMillan, R. P.; Hulver, M. W.; Brown, D. A.; Tessem, J. S.; Neilson, A. P. Common gut microbial metabolites of dietary flavonoids exert potent protective activities in β-cells and skeletal muscle cells. *J. Nutr. Biochem.* **2018**, *62*, 95−107.
(41) Yan, D.; Fan, P. C.; Sun, W. L.; Ding, Q. Z.; Zheng, W.; Xiao, W. D.; Zhang, B. W.; Zhang, T.; Zhang, T.; Shi, J. H.; Chen, X. J.; Chen, P. R.; Zhang, J.; Hao, Y.; Sun, X. G.; Pang, X.; Dong, Y. S.; Xu, P.; Yu, L. Y.; Ma, B. P. Anemarrhena asphodeloides modulates gut microbiota and restores pancreatic function in diabetic rats. *Biomed. Pharmacother.* **2021**, *133*, 110954.
(42) Kaźmierczak-Siedlecka, K.; Vitale, E.; Makarewicz, W. COVID-19 - gastrointestinal and gut microbiota-related aspects. *Eur. Rev. Med. Pharmacol. Sci.* **2020**, *24*, 10853−10859.
(43) Chen, Z.; Lv, Y. W.; Xu, H. C.; Deng, L. Herbal Medicine, Gut Microbiota, and COVID-19. *Front. Pharmacol.* **2021**, *12*, 646560.
(44) Zhang, Q.; Yue, S.; Wang, W.; Chen, Y.; Zhao, C.; Song, Y.; Yan, D.; Zhang, L.; Tang, Y. Potential Role of Gut Microbiota in Traditional Chinese Medicine against COVID-19. *Am. J. Chin. Med.* **2021**, *49*, 785−803.
(45) Li, Q.; Nie, J.; Wu, J.; Zhang, L.; Ding, R.; Wang, H.; Zhang, Y.; Li, T.; Liu, S.; Zhang, M.; Zhao, C.; Liu, H.; Nie, L.; Qin, H.; Wang, M.; Lu, Q.; Li, X.; Liu, J.; Liang, H.; Shi, Y.; Shen, Y.; Xie, L.; Zhang, L.; Qu, X.; Xu, W.; Huang, W.; Wang, Y. SARS-CoV-2 501Y.V2 variants lack higher infectivity but do have immune escape. *Cell* **2021**, *184*, 2362−2371.
(46) Kabinger, F.; Stiller, C.; Schmitzová, J.; Dienemann, C.; Kokic, G.; Hillen, H. S.; Höbartner, C.; Cramer, P. Mechanism of molnupiravir-induced SARS-CoV-2 mutagenesis. *Nat. Struct. Mol. Biol.* **2021**, *28*, 740−746.
(47) Yin, W.; Mao, C.; Luan, X.; Shen, D.; Shen, Q.; Su, H.; Wang, X.; Zhou, F.; Zhao, W.; Gao, M.; Chang, S.; Xie, Y.; Tian, G.; Jiang, H.; Tao, S.; Shen, J.; Jiang, Y.; Jiang, H.; Xu, Y.; Zhang, S.; Zhang, Y.; Xu, H. E. Structural basis for inhibition of the RNA-dependent RNA polymerase from SARS-CoV-2 by remdesivir. *Science* **2020**, *368*, 1499−1504.
(48) Huang, K.; Zhang, P.; Zhang, Z.; Youn, J. Y.; Wang, C.; Zhang, H.; Cai, H. Traditional Chinese Medicine (TCM) in the treatment of COVID-19 and other viral infections: Efficacies and mechanisms. *Pharmacol. Ther.* **2021**, *225*, 107843.
(49) Ren, W.; Liang, P.; Ma, Y.; Sun, Q.; Pu, Q.; Dong, L.; Luo, G.; Mazhar, M.; Liu, J.; Wang, R.; Yang, S. Research progress of traditional Chinese medicine against COVID-19. *Biomed. Pharmacother.* **2021**, *137*, 111310.
(50) Xin, S.; Cheng, X.; Zhu, B.; Liao, X.; Yang, F.; Song, L.; Shi, Y.; Guan, X.; Su, R.; Wang, J.; Xing, L.; Xu, X.; Jin, L.; Liu, Y.; Zhou, W.; Zhang, D.; Liang, L.; Yu, Y.; Yu, R. Clinical retrospective study on the efficacy of Qingfei Paidu decoction combined with Western medicine for COVID-19 treatment. *Biomed. Pharmacother.* **2020**, *129*, 110500.
(51) Deng, J.; Ma, Y.; He, Y.; Yang, H.; Chen, Y.; Wang, L.; Huang, D.; Qiu, S.; Tao, X.; Chen, W. A Network Pharmacology-Based Investigation to the Pharmacodynamic Material Basis and Mechanisms of the Anti-Inflammatory and Anti-Viral Effect of Isatis indigotica. *Drug Des., Dev. Ther.* **2021**, *15*, 3193−3206.
(52) Lin, Y.; Shen, C.; Wang, F.; Fang, Z.; Shen, G. Network Pharmacology and Molecular Docking Study on the Potential Mechanism of Yi-Qi-Huo-Xue-Tong-Luo Formula in Treating Diabetic Peripheral Neuropathy. *J. Diabetes Res.* **2021**, *2021*, 9941791.

https://doi.org/10.1021/acsomega.2c04589
ACS Omega 2022, 7, 36598−36610